Quantum Science and Technology

PAPER • OPEN ACCESS

Landau level single-electron pumping

To cite this article: E Pyurbeeva *et al* 2025 *Quantum Sci. Technol.* **10** 045013

IOP Publishing Quantum Sci. Technol. 10 (2025) 045013 https://doi.org/10.1088/2058-9565/adf6d3

Quantum Science and Technology

RECEIVED
14 February 2025

REVISED
17 July 2025

ACCEPTED FOR PUBLICATION
1 August 2025

PUBLISHED
12 August 2025

PAPER

Landau level single-electron pumping

E Pyurbeeva[1,2,*], M D Blumenthal[3,*], J A Mol[2], H Howe[4], H E Beere[5], T Mitchell[5], D A Ritchie[5] and M Pepper[4]

[1] Fritz Haber Center for Molecular Dynamics, Institute of Chemistry, The Hebrew University of Jerusalem, Jerusalem 91904, Israel
[2] School of Physical and Chemical Sciences, Queen Mary University of London, Mile End Road, E1 4NS London, United Kingdom
[3] Department of Physics, University of Cape Town, Rondebosch, Cape Town 7700, South Africa
[4] University College London, London Centre for Nanotechnology and Department of Electrical Engineering, WC1A 0AH London, United Kingdom
[5] University of Cambridge, Physics Department, Cavendish Laboratory, CB3 0HE Cambridge, United Kingdom
[*] Authors to whom any correspondence should be addressed.

E-mail: eugenia.pyurbeeva@mail.huji.ac.il and mark.blumenthal@uct.ac.za

Keywords: electron pump, metrology, quantum dot, quantum Hall effect, Landau levels, 2DEG, spin

Supplementary material for this article is available online

Abstract

We present a detailed study of the effect of a strong perpendicular magnetic field on single-electron pumping in a device utilising a finger-gate split-gate configuration, characterised by high pumping precision. In the quantum Hall regime, we demonstrate electron pumping from Landau levels in the leads, where the measurements exhibit pronounced fluctuations in the lengths of the pumping plateaus with magnetic field, reminiscent of Shubnikov–de Haas oscillations. In order to explain this similarity, we introduce a new physical model for the dynamics of the operation of a single-electron pump. We show that the pumping process is dependent on the density of states of the 2D electron gas in the leads within a single narrow energy window. Applying our model to experimental data allows for the determination of physical parameters of the pump and its operation; such as the capture energy of the electrons, the broadening of the quantised Landau levels in the leads, and the quantum lifetime of the electrons.

1. Introduction

Technological applications, such as quantum information processing, nano-electronics, and electron quantum optics require the control of individual electrons with a high degree of accuracy [1–17]. AlGaAs high frequency single-electron pumps [18, 19] as well as silicon pumps [20–22] capable of delivering quantised charges, have been extensively studied for this purpose in the past decades, with considerable advancements made [23, 24]. Much effort has been spent on improving the accuracy of these pumps [25–28], with new efforts to utilise machine learning to characterise the pumps [29]. In this paper we examine the pumping mechanism itself when operating in the quantum Hall regime, paying particular attention to the capture process during the pump cycle. In the characterisation of deterministic single-electron pumps, the universal decay cascade (UDC) model presented in the seminal work by Kashcheyevs *et al* [30] remains the only paradigm. Its main result is the equation [30, 31]:

$$I = ef\sum_{n} \exp\left[-\exp\left(-\alpha_n\left(V_{\text{exit}}-\delta_n\right)\right)\right] \tag{1}$$

which gives good agreement with experimental data and allows for the determination of a set of parameters α_n, δ_n (where n is the plateau number), acting as a 'fingerprint' quantifying the accuracy and dynamics of an individual device. The model, however, is limited in its ability to explain experimentally observed physical phenomena. This limitation needs to be overcome as more complex devices are utilised as electron pumps [32].

We present experimental observation of a split-gate finger-gate (SFG) electron pump [31] operating in a perpendicular magnetic field. The evolution of the pumped current is studied as the magnetic field is swept from 1 to 9 T. We aim to interpret the behaviour of the field-dependent pumped current in terms of the well established theory of Landau levels allowing for the extrapolation of experimental properties such as the quantum lifetime of the electrons and capture energy during the pump cycle. Some studies of the effect of a magnetic field on electron pumping have suggested monotonic lengthening of the pumping plateaus, and thus increased pumping precision [33–37]. Fletcher *et al* [36] attributed this to the increased sensitivity of tunnelling rates to the potential profile and the suppression of back tunnelling. Others [38, 39] observed oscillations of the plateau lengths, which Leicht *et al* [38] compared to the Hall resistance of the pump as a function of magnetic field, implying a role of the Landau level quantisation of the leads to pumping.

Our observations, making use of the high precision of the SFG pump configuration [31], show dramatic oscillations of the plateau length, closely correlated with the Shubnikov–de Haas (SdH) oscillations we measure in the same device. We thus assume that the density of states in the leads holds the dominant role, while other effects of the magnetic field [36] constitute an additional weaker dependence.

This allows us to introduce a new physical model for the operation of the pump, which is in agreement with the results of the UDC model, and separates the individual properties of the device from the effect of the magnetic field. It gives new insight into the dynamics of the pumping process, describes the data qualitatively and allows us to determine the capture energy of the pump and the electrons' quantum lifetime.

2. Experiment

The SEM image of the pump and the schematic of the experiment are shown in figure 1(a), with further details on fabrication and measurement given in the Methods section. The pump in our experiment was run at constant RF amplitude ($V_{\mathrm{Amp}} = 300$ mV), frequency ($f_{\mathrm{RF}} = 180$ MHz), entrance gate DC offset voltage ($V_{\mathrm{ent}} = -600$ mV) and source–drain bias ($V_{\mathrm{SD}} = 100$ mV). The magnetic field B and the exit gate voltage V_{exit} were set as variable parameters. Figure 1(b) shows a pumpmap [40] of the current as a function of V_{exit} and B.

The principle of device operation is illustrated in figure 1(c) (i)–(iv), which shows the time evolution of the cross-section of the spatial 3D potential created by the gates (we show $e\varphi$, the negative of the electrostatic potential, illustrating the potential energy of electrons). At the beginning of the cycle (i), the left entrance barrier is low and the dot potential profile has a single maximum. As the entrance barrier potential increases (ii), a local minimum appears in the potential, creating confined states which can exchange and become occupied with electrons from the source (capture stage). With further increase of left barrier height (iii), the confined states become isolated from the source and move with the evolution of the potential profile. Here, no further electrons can enter the dot and the decay of electrons back to the source is suppressed. Finally (iv), the confined states are destroyed and all electrons are ejected into the drain.

We note that figure 1(c) merely illustrates the configuration of the electrostatic potential energy of the pump. The number of pumped electrons per cycle at constant RF frequency and amplitude depends on both the DC gate voltages, as well as the magnetic field (figure 1(b). Here we have tuned the pump into a regime where the DC voltage and RF on the exit gate ensure that the electrons are always ejected and we only concern ourselves with the capture process during the pump cycle. Exploring the capture process is the primary focus of the paper.

Figure 1(d) shows four pumping traces at different magnetic fields for a fixed entrance gate offset voltage and RF parameters. The pumped current evolves as a function of the exit gate voltage V_{exit}, with the integer number of pumped electrons increasing as the DC voltage on the exit barrier is made more positive (the barrier is lowered) – this is a common feature of electron pumping [18, 19].

As a function of magnetic field, the first three traces in figure 1(d) show a trend towards plateau lengthening, in agreement with previous studies [33, 34]. The plateau length dependence is however non-monotonic, as can be seen from the 8 T trace, but instead oscillatory. This behaviour is further emphasised in figure 1(b), a full magnetic field dependent pump map, where a dramatic resonance peak at around 7.2 T is visible.

These oscillations are reminiscent of magnetic field dependencies seen in the SdH effect, similarly to the Hall resistance in Leight *et al* [38] To make a comparison, we study the SdH effect in the pump by measuring the longitudinal resistance of the device as a function of magnetic field, first with the finger gate grounded (figure 1(e), orange) and then with an RF signal on the finger gate (figure 1(e), turquoise) with the parameters of the RF signal set as used during pumping.

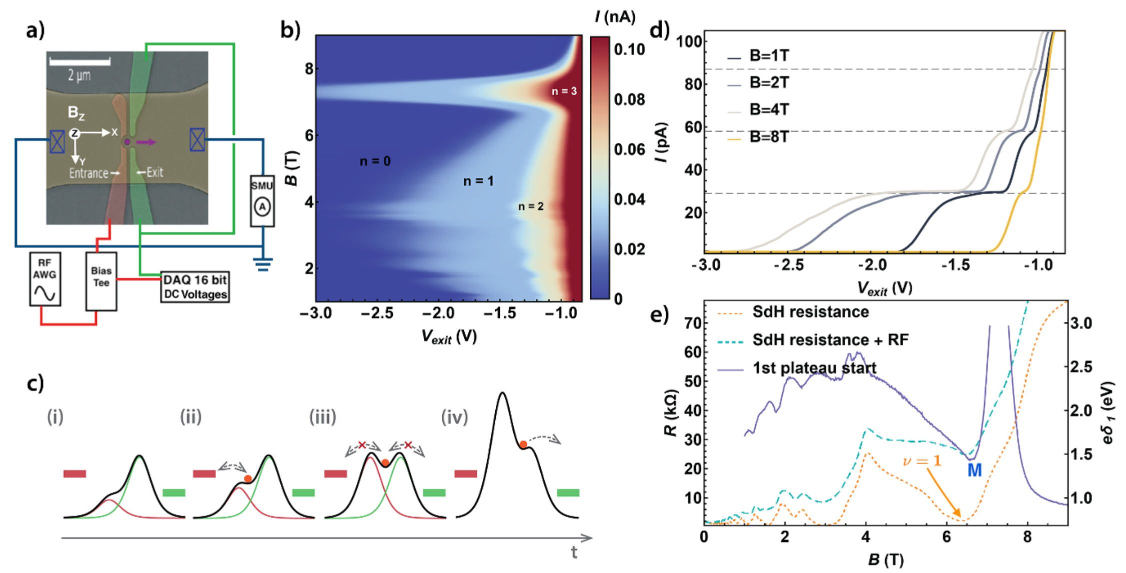

Figure 1. (a) A false colour SEM image of the SFG device with experimental set-up. Two terminals are shown, however the device contains a four terminal Hall geometry allowing for routine measurement of the quantum Hall effect and SdH. (b) 2D colour map showing the dependence of the pumped current on the magnetic field B and exit voltage V_{exit}. (c) A set of schematics illustrating a single pump cycle in a SFG pump. The red and green profiles show the potential energy profiles created by the source/drain electrode, and the thick lines the Fermi levels of the corresponding bath (following the colour scheme in panel (a). (i) At low momentary values of $eV_{\mathrm{ent}}(t)$ the potential profile presents a single maximum, preventing direct current from the source to the drain. (ii) As $eV_{\mathrm{ent}}(t)$ increases, confined states form in the potential profile, and exchange electrons with the source. (iii) Further increase of $eV_{\mathrm{ent}}(t)$ isolates the confined electron(s) from both the source and the drain, such that no further electron can enter or decay from the QD. (iv) All confined states are destroyed and electrons are deposited into the drain. (d) Pumping traces in V_{exit} for several values of B. The lengthening of the plateaus can be observed initially, in agreement with previous work [31], but it is not monotonic in B. (e) The starting voltage of the first plateau, $e\delta_1$ (solid purple) vs. the Shubnikov–de Haas effect in the same sample with RF excitation on the finger-gate (dashed turquoise) and without (dashed orange).

The purple plot in figure 1(e) shows the potential energy barrier height (absolute value of the exit gate voltage) corresponding to the start of the first pumping plateau (current is at $\mathrm{e}^{-1} \approx 0.37$, where e is the natural exponent, of the expected plateau value, see equation (1)) as a function of magnetic field. While the three plots in figure 1(e) are far from identical, there is significant similarity in their peak structures that requires explanation.

As the magnetic field oscillations in the SdH effect originate in the Landau quantisation of the electron states, we make the conjecture that similarly, the pumping of electrons is largely defined by the density of states in the source of the pump. The difference between the pure SdH signal (figure 1, orange) and the first plateau starting potential (figure 1, purple) can be explained by the presence of RF signal (figure 1, turquoise), as well as the exact mechanism of pumping. The change in electron density observed when comparing the orange and turquoise plots is attributed to the voltage applied by the RF signal generator to the finger gate. This voltage locally modifies the electron density, either increasing or decreasing it depending on the specific characteristics of the applied signal. In this experiment, we replicate the RF signal used during the pump cycle, which generates an overall potential profile averaged over the full RF cycle. This profile results in a depletion of electrons. There is also present an expected increase in the longitudinal resistance. This is due to the reflection of one or more edge states by the RF gate [41].

The model and quantitative data analysis to follow expands on this experimental observation.

3. The model

3.1. Motivations

A single-electron pump is a complex open quantum system incorporating both particle and energy exchange, a time-dependent Hamiltonian, multiple competing time-scales, out-of-equilibrium conditions and multi-electron processes, all of which make it a serious challenge for theoretical description [42]. Combinations of these effects are studied in topics such as far-from-equilibrium thermodynamics in nanodevices [43], as well as in applications of driven quantum dots such as quantum heat engines and refrigerators [44–47].

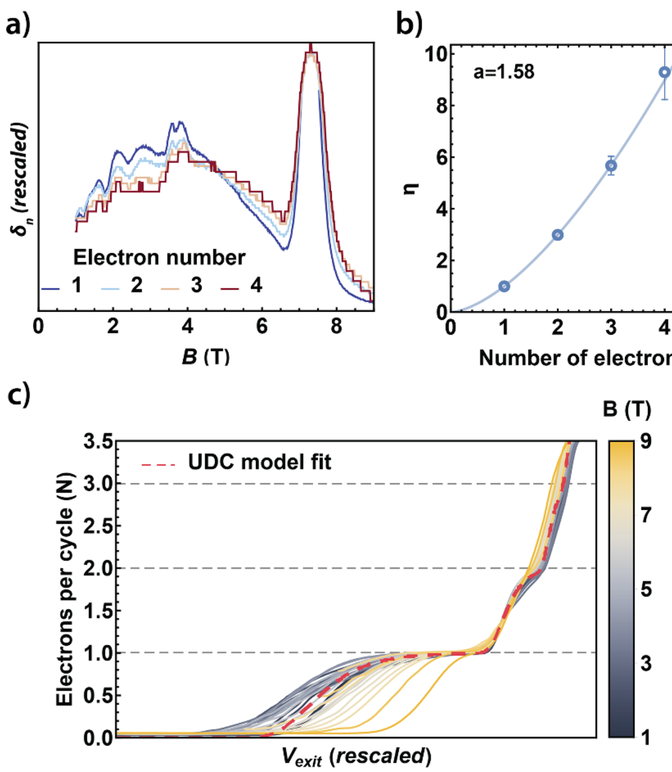

Figure 2. (a) The pumping onset voltage δ_n for the first four plateaus ($n = 1\ldots4$) linearly scaled to coincide with each other. (b) The calculated scaling factors of δ_1–δ_4. (c) Pumped current vs. V_{exit} for varying magnetic fields from $B = 1$ T to $B = 9$ T in 0.5 T steps, horizontally rescaled by the magnetic field-dependent parameter $\lambda(B)$. Red dashed line shows the UDC fit to the averaged trace.

Single-electron pumps also exhibit additional complexity due to qualitative changes, such as the creation and destruction of confined states, as well as strong system-bath coupling associated with it. Quantitative changes, such as the cycling of addition energy further complicate the system.

The double-exponential fitting equation for the pumping curves [31] of the UDC model (equation (1)) is the primary theoretical approach to the description of single-electron pumps. It gives a good fit to the pumped current in a wide variety of electron pump geometries [31] and allows to compare devices operating in identical experimental conditions. Despite later expansions [48, 49] on the model, alternative proposals, such as the Sudden Decoupling Theory [50–52], and attempts at a dynamical analysis of the system [53], there is currently no well-established link between the 'fingerprint' coefficients α_n, δ_n and the key physical parameters, such as temperature, magnetic field, RF signal amplitude, or frequency. Such a connection can be found from the explicit consideration of a physical model. Recent work [54] performed a dynamical analysis for a driven quantum dot from an open quantum system perspective, including a study on two-electron emission processes, however such approaches are computationally involved and highly model-dependent.

We propose a qualitative and intuitive approach, using experiment as a starting point. Our experimental data (figure 1(b)) provides a systematic high-precision study of the dependence of quantised pumping on the magnetic field. Our observations serve as a basis for developing a physical model of the dynamics of the electron pump.

3.2. Empirical observations

Before constructing a model, we further detail our experimental observations. Figure 1(e) compares the onset of pumping of the first plateau as a function of V_{exit} (dark blue), which corresponds to the current reaching $\mathrm{e}^{-1} \approx 0.37$ of the true expected integer plateau, where e is the natural exponent, to the SdH resistance in B—turquoise (with RF) and orange (No RF). The pump map in figure 1(b) shows the same peak pattern for all plateaus ($n = 1,2,3,4$).

We proceed with a direct comparison of the first four plateaus. In figure 2(a) we plot the onset voltages for the first four pumping plateaus, δ_1–δ_4 (voltage points from $n = 1$ (blue) to $n = 4$ (red) as a function of B, linearly scaled to minimise the sum of the squares of differences between the corresponding data points from each pump plateau for all B. The scaling factors $\eta(n)$ follow a power law in $\eta(n) \approx n^a$ with $a = 1.58$.

δ_1–δ_4 coincide (overlap of all curves in figure 2(a)) up to a linear transformation indicating that all pumped plateaus follow the same oscillatory pattern reminiscent of the SdH oscillations, instead of a separate magnetic field dependence for each δ_n. The pump plateaus all dilate in the same way, either contracting or expanding in V_{exit} as the magnetic field is varied.

This allows us to introduce a single parameter $\lambda(B)$ governing the overall length of the pumping trace, such that the UDC equation (equation (1)) can be written as:

$$I = ef \sum_n \exp\left[-\exp\left(-\alpha_n \left(V_{\text{exit}} - \lambda\left(B\right)\delta_n'\right)\right)\right] \tag{2}$$

where the coefficients δ_n' are magnetic field-independent.

To further substantiate our claim that the entire pump map is represented as a single pumping trace dilating and contracting with magnetic field as a whole, we present figure 2(c), which shows pumping traces at different magnetic fields dilated by $\lambda(B)$ coinciding in their plateau positions, with the exception of the high field traces. Additionally, figure 2(c) shows the UDC fit (dashed red) to the average of the pumping traces, which comprises the pumping trace inherent to the device at $B = 0$ with $\lambda(0) = 1$ and the experimental conditions„such as frequency and temperature, remaining constant. The pump traces shown here are taken from a pump map operating in the UDC regime. For a full V_{ent} vs V_{ext} pump map of this device please refer to the following papers [24, 31] where the same device was measured.

From these experimental observations, we can thus conclude that the magnetic field dependence of pumping can be described as that of a single device-dependent pumping trace, dilating and contracting with magnetic field by the length factor $\lambda(B)$. This dilation strongly resembles the SdH oscillations of longitudinal resistance of the 2DEG, which is proportional to the density of states at the Fermi-level (figure 1(e)).

3.3. The 0-DIP model and dot parameters

We now propose a physical model explaining our experimental observations.

The main physical premise of the UDC model [30] is that the quantum dot is 'loaded' with electrons while its energy levels are beneath the Fermi level, and once the quantum dot is energetically raised above it, non-equilibrium relaxation, or backtunnelling, occurs until some number of electrons remain to be pumped into the drain. However, this is not corroborated by our experiment.

Electron pumping is inherently governed by electron exchange between a 2DEG and a quantum dot. Such processes are commonly dependent on the density of states in the electrode [55], which, in our case, can be seen in the SdH resistance. However, the sharp Landau level signatures in $\lambda(B)$, the overall trace length factor, can only be observed if all electron exchange processes determining the pumping at a given magnetic field are confined to an energy window much narrower than the width of the Landau level, in contradiction to the usual description of the UDC model.

To explore the physical nature of electron pumping and explain the origin of this energy confinement of electron exchange, we first assume that for the electrons in the pump, the leading term in energy is due to the electrically defined potential of the pump, with the magnetic field-dependent contribution being a small correction to it. Thus, we begin with the analysis of a 1D model of the electron potential energy profile.

When voltages V_{ent} and V_{exit} are applied to the entrance and exit electrodes, the potential energy profile $E(x)$ is a sum of two smooth differentiable peak functions $E_{\text{ent}}\varphi_{\text{ent}}(x)$ and $E_{\text{exit}}\varphi_{\text{exit}}(x)$. The peak maxima are given by E_{ent} and E_{exit}, which depend linearly on the voltages applied (figure 3(a)) and $\varphi_{\text{exit}}(x)$ and $\varphi_{\text{ent}}(x)$ are the dimensionless spatial potential profile functions with maximum values of 1. If the peaks are sufficiently close to one another, for every value of E_{exit} there exist a value of E_{ent} for which the total potential profile exhibits an inflection point with a zero derivative on the source side of the potential profile. We call this configuration (figure 3(b)) the *0-DIP potential* (for 'zero derivative inflection point'). The value of the inflection point energy at the the 0-DIP potential configuration is proportional to E_{exit} (and therefore V_{exit}), where we define the proportionality coefficient as α.

The significance of the 0-DIP potential is that it approximately separates two configurations of the dynamically defined dot—that with no confined electron states, and that containing one or multiple confined states. We assume that the first confined state forms in a 'shallow' potential, making both the energy E_c at which it first forms and the corresponding E_{ent} close in value to the inflection point αE_{exit}. A crucial point in our model is that a further increase of E_{ent} during the RF cycle leads to a rapid reduction in the tunnel coupling between the now-formed confined states and the source (figure 3(c)), and after a small increment dE in entry barrier height, the dot is effectively completely isolated, not only from the drain, but also from the source (grey shaded profile in figure 3(b)). This means that E_c, the energy of the formation of the first confined state can be thought of as the capture energy, since all electron exchange processes occur within a narrow energy window after this energy as indicated in figure 3(b) by the blue shaded strip.

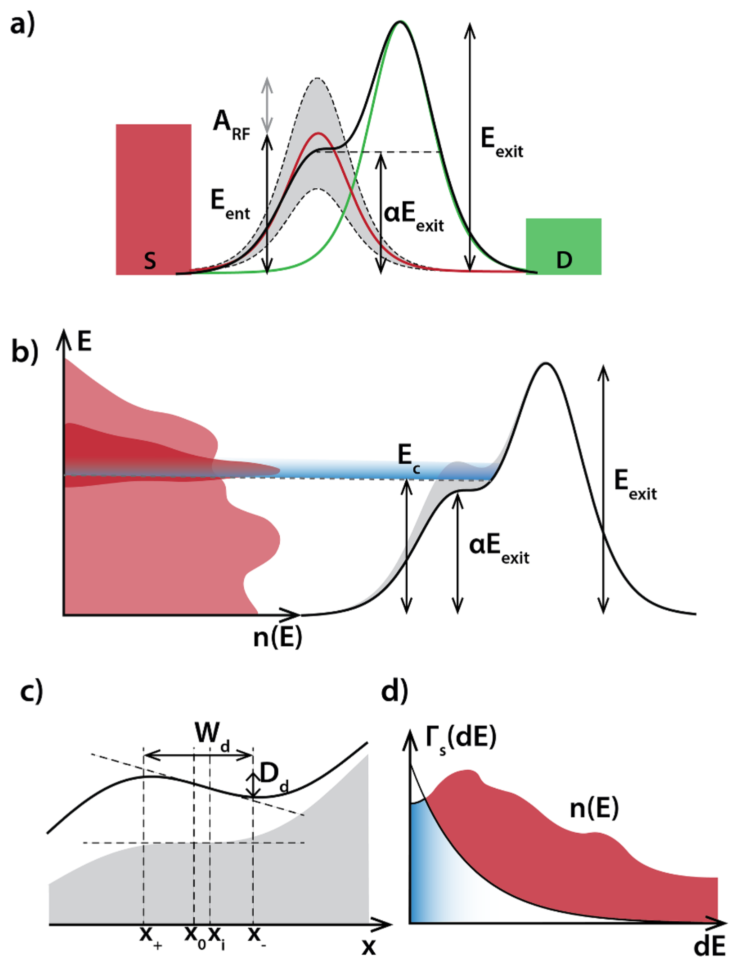

Figure 3. (a) A labelled schematic of the potential profile parameters. The green and red peaks show the exit potential profile and the constant offset of the entrance potential respectively. The black curve is the 0-DIP potential, realised at one of the momentary values of E_{ent}, which lie within the grey shaded area with the width being the amplitude of the RF signal A_{RF}. (b) The device potential profile in the vicinity of the 0-DIP configuration. As E_{ent} goes past the the 0-DIP configuration (the grey shaded profile), the first confined state appears at E_{c}, after which the coupling with the source falls exponentially. All electron exchange processes occur within the blue shaded energy range. The shaded red profiles show an arbitrary density of states dependences, weak (pale red) or strong (dark red) in energy. (c) Schematic showing the zoomed-in region of the QD potential close to the 0-DIP point with the length scale dimensions (W_{d} width, and D_{d} depth) indicated. The grey area indicates the 0-DIP configuration. x_+ and x_- are the local maximum and minimum respectively, x_i is the inflection point, x_0 is the inflection point in the 0-DIP configuration. (d) The schematic showing the change in tunnel rate Γ and an arbitrary source electron density $n(E)$ as the energy of the entrance barrier is changed (dE).

To substantiate this claim, we define two fundamental dimensions of the dot: W_{d}—the width of the entrance potential barrier and the characteristic size of the dot (the distance between the local minimum and maximum in the potential profile, $x_- - x_+$ in figure 3(c), and D_{d}—the depth of the dot and the height of the potential barrier (the potential energy difference between x_- and x_+), and study their evolution as a function of dE in a one-dimensional system close to the 0-DIP point. Analytically making use of Taylor expansion (see Methods) we find the following two expressions for the effect of the potential energy profile parameters on the dot shape:

$$\begin{cases} W_{\mathrm{d}} = C_W\sqrt{\frac{\mathrm{d}E}{E_{\mathrm{exit}}}} \\ D_{\mathrm{d}} = C_{\mathrm{D}}\sqrt{\frac{(\mathrm{d}E)^3}{E_{\mathrm{exit}}}} \end{cases} \tag{3}$$

where C_W and C_{D} are energy-independent coefficients.

The effective barrier width and height both increase with dE, as the pump goes past the 0-DIP configuration. And since the coupling between the confined states in the dot and the source falls exponentially with both W_{d} and D_{d}, the result serves as further support for the claim that the dot is only coupled to the source in a narrow energy window (figure 3(d)). While the exact form of the dependence will be different for a two-dimensional case and will depend on the geometry of the electrodes, qualitatively it will follow the 1D case. Additionally, an increase of W_d with lower E_{exit} agrees with more electrons per cycle being pumped with less negative V_{exit}.

We note that the different physical model is not in contradiction with the results of the UDC model, as equation (1) does not change with the range of energies at which back-tunnelling occurs. Furthermore, we are not attempting to describe the exact dynamics of electrons around the 0-DIP point, between the formation of confined states and the quantum dot being decoupled from the source—such work can form a separate study. We simply claim that however complex the exchange dynamics, they are limited to a small energy window, and can be used to probe the density of states in the source, as the capture probability depends on it.

Figure 3(b) shows the energy profile of the pump close to the 0-DIP point and a source with an arbitrary density of states. A change in E_{exit} leads to two effects—a change in the inflection point, αE_{exit}, and therefore capture energy E_c, and a change in the size of the dot, and therefore the probability of capture. Since the pumping trace length is a function of magnetic field B only, we can conclude that the first effect is not significant and the change of capture energy over our line scan is small compared to the width of the Landau level (if it were not the case, we could observe a decrease of the number of pumped electrons with an increase of exit voltage, see figure 3(b), dark red). This means that any change in the capture energy throughout the experiment is small in comparison to the width of the Landau level.

An important distinction is that while in our model pumping depends on the density of states at the capture energy, the SdH resistance gives the density of states at the Fermi energy, which is a function of magnetic field. This will be the source of some misalignment between the data in figure 1(e).

4. Quantitative data analysis

In our 0-DIP model, we assume that successful electron capture by the quantum dot occurs when the dot's capture energy, E_c, is resonant with an occupied Landau level in the source reservoir. Once capture has taken place, the quantum dot decouples rapidly from the source over a narrow energy bandwidth.

To validate our assumptions in the 0-DIP model, we investigate the correlation between the dynamics of the density of states of the Landau levels in the source at the capture energy, with the oscillatory behaviour of the pumped current in B. A direct calculation of current would require additional assumptions about the dynamics at capture. We aim to investigate how the probability of capture is increased with a corresponding increase in the density of states in the source that leads to an enhancement in robustness of pumped current in V_{exit} as seen in figure 4(b) (red trace).

The Landau level energies including spin are quantized according to

$$E_n = \left(n + \frac{1}{2}\right)\hbar\omega_c \pm \mu_B Bsg, \tag{4}$$

where $\omega_c = \frac{eB}{m^*}$ denotes the cyclotron frequency, the $\pm$ for spin up and down respectively, e is the elementary charge, B is the magnetic field strength, m^* the effective electron mass, $\mu_B = \frac{e\hbar}{2m^*}$ the Bohr magneton, S the spin factor($s = \frac{1}{2}$ for electrons) and g the Landé g-factor ($g = 1$). The degeneracy per unit area, or the density of states, associated with each Landau level is given by

$$n_B = \frac{eB}{h}. \tag{5}$$

The density of states given here is assuming the Landau level is described by the Dirac delta function, which is only the case for an ideal system where scattering is completely ignored [56]. It is more realistic to assume that the electron survives for a finite time, τ_i, between scattering events. τ_i is known as the quantum lifetime–the average time a carrier remains in a momentum eigenstate before scattering [57].

As a consequence, the energy of the Landau level is defined with a precision

$$\Gamma = \frac{\hbar}{\tau_i}. \tag{6}$$

Each Landau level acquires a finite width and can be modelled as a Gaussian with a full width at half maximum (FWHM) denoted by Γ. The states from equation (5) are therefore spread into the area now given by the Gaussian shaped Landau level.

As the magnetic field is increased, both the Landau level energies and the associated density of states increase as well. By tracking these changes in tandem with the Fermi energy E_F—defined here as the maximum electron energy within the topmost occupied Landau level—we compare the field-dependent

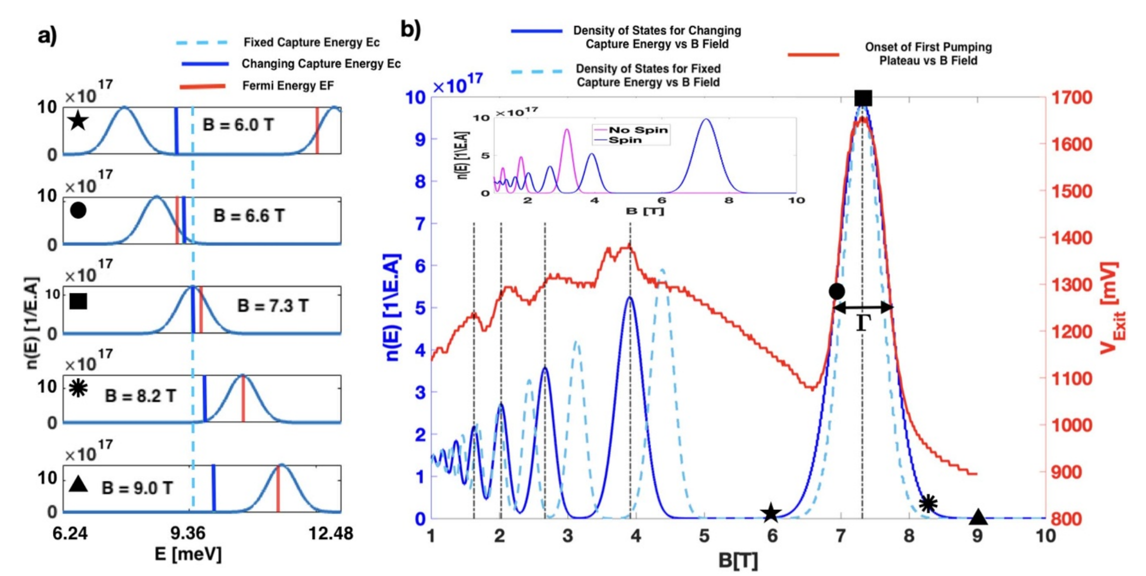

Figure 4. (a) Schematics of the evolution of the spin-split first Landau level for B values chosen around the main resonance peak centred at $B = 7.3$T. The black shape markers indicate the chosen B values on the resonance peak in panel b. The Fermi energy is indicated by the red vertical lines, the turquoise dotted line indicates a fixed capture energy and the blue line a changing capture energy, with B. (b) Onset of 1st plateau pumping (experimental data) in red taken directly from figure 1(e). Blue and turquoise plots indicate the simulated density of states for changing capture energy and fixed capture energy respectively vs B field. Γ shows from where in the experimental data (red) plot the Landau broadening was determined. Inset: density of states for changing capture energy vs B field, shown considering electron spin splitting (blue) and ignoring spin splitting (pink).

evolution of the Landau-level density of states with the experimentally observed magnetic field dependence of the pumped current (figure 1(e), blue trace). A strong correlation between these traces would support the validity of Landau level loading and allow for the extraction of physically meaningful parameters. To quantify the field dependence of the Landau levels and related parameters, the 2DEG electron density n_{D} is needed. We measured n_{D} using the SdH oscillation method. This involved analysing periodic oscillations in the longitudinal resistivity R_{xx} as a function of inverse magnetic field. The electron density was extracted using the expression

$$n_{\mathrm{D}} = \frac{2e}{h} \cdot \frac{1}{\Delta(1/B)}, \tag{7}$$

where $\Delta(1/B)$ is the oscillation period in inverse magnetic field, and the pre-factor of 2 accounts for spin degeneracy in the absence of Zeeman splitting (a valid assumption for $B < 2\,\mathrm{T}$).

Two SdH R_{xx} traces of the pump device were measured at a base temperature below 100 mK: one with all gates of the pump grounded (orange trace in figure 1(e)), and another with the quantum dot pump's finger gate driven at its operational frequency and amplitude (turquoise trace), as described in section 2 . From the grounded trace, we identified resistivity minima at fields $B = 1.050\,\mathrm{T}$ and $B = 1.568\,\mathrm{T}$, and substituted into equation (7) to extract a two-dimensional electron density of

$$n_{\mathrm{D}} = 1.53 \times 10^{15}\,\mathrm{m}^{-2}. \tag{8}$$

This value is in good agreement with the nominal electron density of $1.87 \times 10^{15}\,\mathrm{m}^{-2}$, measured independently by the Cavendish Laboratory at the University of Cambridge. The slight discrepancy is attributed to device fabrication effects, which likely modify the 2DEG properties.

From the SdH trace in figure 1(e) (orange trace) we can determine the B field at which the electrons start to occupy only the lowest Landau level. We make use of the filling factor ν (representing the number of occupied Landau levels), which is defined by

$$\nu = \frac{n_{\mathrm{D}}}{n_{\mathrm{B}}} = \frac{n_{\mathrm{D}} h}{eB}. \tag{9}$$

Setting $\nu = 1$ for the occupation of only the first Landau level, we find $B = 6.36\,\mathrm{T}$. This corresponds with the final SdH minimum (see orange trace with arrow in figure 1(e)(where the Fermi energy sits in an localised state above the first full Landau level) as well as the minimum in pumped current marked by an M in figure 1(e) (blue trace).

This field value will be of use in estimating the capture energy of the dot as detailed later in this section.

We next extract the Landau level broadening Γ, as defined in equation (6), from the FWHM of the resonance peak in figure 1(e) (blue trace), which is replotted for clarity in figure 4(b) (red trace). From this analysis, we obtain $\Gamma = 0.84\,\mathrm{meV}$, corresponding to a quantum lifetime $\tau_i = 0.78\,\mathrm{ps}$, consistent with values previously reported in the literature [58–60]. In the pumping regime, the application of an RF signal introduces additional scattering mechanisms that are expected to reduce the quantum lifetime. A detailed investigation of the dependence of τ_i on RF frequency and amplitude is a subject for future study.

The above method used to determine Γ is supported by the observation that the minimum in pumped current occurs at $B = 6.36\,\mathrm{T}$, coinciding with the condition $\nu = 1$ in the orange SdH trace, where the Fermi energy lies in a region of low density of states. We attribute the observed oscillations in pumped current as a function of magnetic field, to the modulation of the density of states in the source lead at the capture energy. Specifically, an increased density of states enhances the likelihood of electron capture, resulting in a broader plateau in pumped current versus V_{Exit}, while a reduced density of states suppresses capture, leading to a decrease in current plateau length. The resonance in pumped current observed at $B = 7.3\,\mathrm{T}$ (indicated by the black square in figure 4(b) is therefore interpreted as corresponding to a maximum in the density of states at the capture energy. This therefore requires the capture energy to align with the centre of the first Landau level. We will attempt later in this section to validate this assumption for the full range of B field from $1-9\,\mathrm{T}$.

Therefore, applying equation (4) with $n = 1$ at $B = 7.3\,\mathrm{T}$, we estimate the capture energy of the pump dot

$$E_{\mathrm{c}} = 9.4\,\mathrm{meV}. \tag{10}$$

We assume first that this capture energy is independent of magnetic field.

Using `MATLAB`®, we calculate the density of states in the source lead at E_{c} over the magnetic field range $B = 1-9\,\mathrm{T}$, shown as the dotted turquoise trace in figure 4(b). On the same axes, we re-plot the onset of the first current plateau (from figure 1(e), blue trace) now the red trace. The comparison reveals some correlation between the oscillatory structure in the pumped current and the density of states at constant E_{c}.

In an attempt to improve on this, we instead calculate the capture energy as a field-dependent quantity $E_{\mathrm{c}}(B)$, assuming in the first-instance a linear dependence across the full magnetic field range. This captures potential magnetic confinement effects in the quantum dot, leading to a changing energy of the first confined state beyond the inflection point. We scale E_{c} from a value of $9.42\,\mathrm{meV}$ at $B = 7.2\,\mathrm{T}$, varying linearly by $\Delta E_{\mathrm{c}} = 2.4\,\mathrm{meV}$ over the full B range. This corresponds to $E_{\mathrm{c}} = 7.5\,\mathrm{meV}$ at $1\,\mathrm{T}$ and $E_{\mathrm{c}} = 9.9\,\mathrm{meV}$ at $9\,\mathrm{T}$, in steps of $\Delta B = 9.0\times10^{-4}\,\mathrm{T}$. The resulting density of states trace (dark blue line in figure 4(b) exhibits strong correlation with the pumped current, as highlighted by vertical dotted lines marking aligned oscillation peaks. For completeness we model the same density of states for a changing energy in B but now ignoring spin. Here we set the second term in equation (4) to zero and assume no lifting of the degeneracy in each Landau level for all B. The result is given in the inset in figure 4(b), no spin—pink trace, along with the inclusion of spin—blue trace. A clear difference is visible, indicating spin effects are essential in modelling the pump behaviour in magnetic field and need to be accounted for.

Despite the improved agreement arising from the linear dependence of $E_{\mathrm{c}}(B)$ on B, successful electron capture still requires that the source resonant Landau level is occupied. To verify whether this holds true in our calculation, we examine the evolution of the broadened Landau levels alongside the Fermi energy E_{F}, modelling as discussed earlier each Landau level as a Gaussian with a FWHM of $\Gamma = 0.84\,\mathrm{meV}$. Figure 4(a) illustrates the spin-split first Landau level ($n = 1$) for selected magnetic field values taken from the resonance peak of the pumped current as indicated by the solid black shape markers. The red vertical lines denote the position of the Fermi energy E_{F}. We compute E_{F} at $T = 0\,\mathrm{K}$ by noting that the total area under the Landau levels up to E_{F} must equal the measured two-dimensional electron density $n_{\mathrm{D}} = 1.53\times10^{15}\,\mathrm{m}^{-2}$. Using equation (5) to include the B dependency in the Landau levels density of states, we integrate the Gaussian-shaped density of states as a function of energy for each magnetic field and determine E_{F} as the energy at which the cumulative area equals n_{D}. This approach enables a field-dependent determination of E_{F}, which is then used to evaluate the occupation of the Landau levels as the magnetic field is varied.

In figure 4(a), the turquoise dashed vertical line indicates the fixed capture energy E_{c}, while the solid blue vertical line shows the changing capture energy in B, $E_{\mathrm{c}}(B)$. At $B = 7.3\,\mathrm{T}$, the Fermi level lies within the lowest Landau level, confirming that all electrons reside in the $n = 1$ state. As B increases from 6 to 9 T, the varying capture energy $E_{\mathrm{c}}(B)$ scans through the first Landau level. At $B = 6\,\mathrm{T}$ the capture energy is in the extended state of the Landau level with a low density of states (figure 4(a) (star)). This corresponds to a drop in pumped current as shown in the red trace in figure 4(b). As the field is increased and the pumped current increases, the capture energy moves through the Landau level with an increase in density of states, peaking at

$B = 7.3$ T, which corresponds with the resonance of the pumped current, before dropping off again. The black solid shapes on the pumped resonance peak (figure 4(b) red trace) are used to identify the relevant schematic in figure 4(a) showing the corresponding Landau level in the source lead, together with the capture energy and Fermi energy . This simulation indicates that the large pumped resonance peak is due to the changing capture energy $E_c(B)$ probing the first Landau level going through a maximum in density of states as B is swept.

5. Conclusion

Our experimental data of single-electron pumping through a SFG quantum dot at high magnetic fields demonstrates oscillatory behaviour reminiscent of the SdH effect. The inclusion of a split-gate on the exit side of the quantum dot allows for an increase in gate resolution due to a lower lever-arm term [31]. This, with the change in potential profile on the exit side of the quantum dot from a simple Gaussian to a saddle-point potential, has allowed for further probing of the dynamics of these on-demand electron sources.

Our analysis together with a new physical description for the pumping dynamics based on the foundations of the UDC model has allowed for the first reported direct measurement of the capture energy, the broadening of Landau levels in such pump devices and therefore the quantum lifetime of the pumped electrons. This demonstration of single electron pumping in the quantum Hall regime, where electrons are captured from specific Landau levels, shows the capture energy to be independent of the exit gate DC voltage for fixed B field, but a change in the capture energy is observed as the B field itself is varied.

Furthermore, we have demonstrated that the split-gate configuration of the electron pump leads not only to high pumping precision, as shown in previous work [24, 31], but to a narrow energy window for the loading of the pump—narrow enough for individual Landau levels to be resolved. The explicit determination of the capture energy in a single-electron pump based on a 2DEG provides valuable insight into the energetics of the loading process and sets a quantitative benchmark for optimising pump performance. Our finding that the capture energy exhibits a linear dependence on the applied magnetic field highlights the role of Landau level formation and offers a tunable parameter for controlling electron capture with high precision. Additionally, by extracting the quantum lifetime of electrons in the pump, we gain access to de-coherence and scattering time-scales that are critical for understanding non-adiabatic errors and achieving high-fidelity pumping. The observed magnetic field dependence of the pumped current, shown to correlate with the changing density of states in the source lead, establishes a direct link between the pump environment and its charge transfer accuracy. This work is especially relevant for quantum metrology and the development of electron-based quantum technologies, where control of accurate on demand single-electrons is paramount.

Our experimental observation of pumping from a narrow energy band, together with the simple physical description of the pump dynamics can serve as a foundation for future more involved theoretical modelling to explore the effect of other parameters on pumping, such as temperature and frequency.

6. Methods

6.1. Fabrication and experiment setup

Our device comprises a single-electron pump with two Ti/Au gates in a finger-gate split-gate geometry (red and green in figure 1(a) respectively). Only the entrance gate, in our the case the finger-gate, is coupled directly to the Agilent RF signal generator. The pumped current is measured via a Keithley 6430 source-measure unit capable of measuring at the femto-ampere level. DC voltages are applied to the gates via multiple channel 16 bit DAQs. Unlike the earlier pump configurations, in which oscillating voltages have been applied to both the exit and entrance gate [18, 61], we follow a later protocol [19, 62], in which the potential of the exit gate is held constant during the pump cycle, and the entrance gate oscillates due to the RF signal added to the constant potential via a bias T. The gates were fabricated using electron beam lithography with Ti/Au thermally evaporated. The entrance finger gate (red) and split gate (green) are used to define the QD entrance and exit gate respectively. DC voltages were applied to all gates using a NI2969 cDAQ with the RF signal coupled to the exit gate via a bias tee. The RF source used was a HP E4400B driving a simple sinusoidal wave.

The device was fabricated on a two-dimensional high mobility GaAs/$Al_xGa_{1-x}As$ Si-doped electron gas system grown using molecular beam epitaxy. The 2DEG was formed 90 nm below the surface (10 nm GaAs cap, 40 nm Si-doped GaAs/$Al_xGa_{1-x}As$, 40 nm GaAs/$Al_xGa_{1-x}As$ spacer, and GaAs substrate with a carrier density $n = 1.9 \times 10^{11}$ cm^{-2} and mobility $\mu = 1.014 \times 10^6$ cm^2 Vs^{-1}). The 2DEG channel pattern was defined using electron-beam lithography and etched to a depth of 40 nm using wet chemistry. The split gate has a width and gap of 400 nm, whilst the finger gate a width of 150 nm. The pitch of the gates are 200 nm.

The sample contained four AuGeNi ohmic contacts. Two were utilised for measurement of pumped current and four when measuring the SdH effect. The sample was loaded into a Leiden Cryogenics dilution fridge with a base temperature of 7 mK and a 10 T superconducting magnet. The pumped current was measured using a Keithley 6430 source measure unit, which was connected to the drain side of the pump. The source side was grounded.

The SdH plot without the RF signal (figure 1, turquoise) differs from assessment measurements in the same wafer with a standard Hall bar. This difference can be attributed to the geometry of the mesa in the pump deviating substantially from a standard Hall bar geometry. The inclusion of Ti/Au gates as well as the fabrication process itself also affect the wafer, altering the electron density and mobility. The application of the RF signal further influences the magnetic field dependence of the device resistance, however both retain the general peak structure of the signature SdH.

6.2. Dot parameters—analytical consideration

We find the dependence of the quantum dot parameters W_{d} and D_{d}—width of the potential barrier and the dot depth in a 1D case—shortly after the system has passed the 0-DIP configuration. The potential profile $E(x)$ is the sum of the potential profiles of both electrodes:

$$E(x) = E_{\mathrm{ent}}\varphi_{\mathrm{ent}} + E_{\mathrm{exit}}\varphi_{\mathrm{exit}} \tag{11}$$

where φ_{ent} and φ_{exit} are the normalised functions of the potentials creates by each of the electrodes independently, we assume they are smooth, differentiable, with a simple peak, and $\max(\varphi_{\mathrm{ent}}) = \max(\varphi_{\mathrm{exit}}) = 1$.

In the 0-DIP configuration, $E_{\mathrm{ent}} = \alpha E_{\mathrm{exit}}$. If x_0 is the inflection point, then the first and second derivatives of the potential profile in it are equal to zero:

$$\begin{cases} E'(x_0) = \alpha E_{\mathrm{exit}}\varphi'_{\mathrm{ent}}(x_0) + E_{\mathrm{exit}}\varphi'_{\mathrm{exit}}(x_0) = 0 \\ E''(x_0) = \alpha E_{\mathrm{exit}}\varphi''_{\mathrm{ent}}(x_0) + E_{\mathrm{exit}}\varphi''_{\mathrm{exit}}(x_0) = 0 \end{cases} \tag{12}$$

Shortly past the 0-DIP configuration, $E_{\mathrm{ent}} = \alpha E_{\mathrm{exit}} + \mathrm{d}E$, the derivatives at the same point are:

$$\begin{cases} E'(x_0) = \mathrm{d}E\varphi'_{\mathrm{ent}}(x_0) \\ E''(x_0) = \mathrm{d}E\varphi''_{\mathrm{ent}}(x_0) \end{cases} \tag{13}$$

In this case (see figure 3(d)), the potential has three special points—the new inflection point x_i, the local maximum x_+ and the local minimum x_-. Assuming that $\mathrm{d}E$ is small and the special points lie within a small vicinity of the former inflection point x_0 we find the distance between the new and the former inflection points $\mathrm{d}x_i$ in the Taylor expansion. Postulating $E''(x_0 + \mathrm{d}x_i) = 0$, we arrive at:

$$\mathrm{d}x_i = -\frac{\mathrm{d}E\varphi''_{\mathrm{ent}}(x_0)}{\alpha E_{\mathrm{exit}}\varphi'''_{\mathrm{ent}}(x_0) + E_{\mathrm{exit}}\varphi'''_{\mathrm{exit}}(x_0)} \tag{14}$$

At the new inflection point, to the first order,

$$\begin{cases} E'(x_i) = \mathrm{d}E\varphi'_{\mathrm{ent}}(x_0) \\ E''(x_i) = 0 \\ E'''(x_i) = \alpha E_{\mathrm{exit}}\varphi'''_{\mathrm{ent}}(x_0) + E_{\mathrm{exit}}\varphi'''_{\mathrm{exit}}(x_0) \end{cases} \tag{15}$$

Finally, we find the distance between the new inflection point x_i and the maximum and minimum x_+ and x_-. Setting

$$E'(x_i + \mathrm{d}x) = E'(x_i) + E''(x_i)\,\mathrm{d}x + E'''(x_i)\frac{\mathrm{d}x^2}{2} = 0 \tag{16}$$

we arrive at:

$$\mathrm{d}x = \sqrt{-\frac{2\mathrm{d}E\varphi'_{\mathrm{ent}}(x_0)}{\alpha E_{\mathrm{exit}}\varphi'''_{\mathrm{ent}}(x_0) + E_{\mathrm{exit}}\varphi'''_{\mathrm{exit}}(x_0)}} \tag{17}$$

We set $2\mathrm{d}x$, the distance between the local minimum and maximum as the characteristic size of the dot, which is equal to the width of the potential barrier; and the depth of the dot, or the height of the barrier can be found as:

$$D_{\mathrm{d}} = 2E'(x_i)\,\mathrm{d}x + 2E'''(x_0)\,\frac{\mathrm{d}x^3}{6} \tag{18}$$

which yields:

$$D_{\mathrm{d}} = \frac{4}{3}\mathrm{d}E\varphi'_{\mathrm{ent}}(x_0)\sqrt{-\frac{2\mathrm{d}E\varphi'_{\mathrm{ent}}(x_0)}{\alpha E_{\mathrm{exit}}\varphi'''_{\mathrm{ent}}(x_0) + E_{\mathrm{exit}}\varphi'''_{\mathrm{exit}}(x_0)}}. \tag{19}$$

The final dependence on the externally imposed energetic parameters has the form:

$$\begin{cases} W_{\mathrm{d}} = C_W\sqrt{\frac{\mathrm{d}E}{E_{\mathrm{exit}}}} \\ D_{\mathrm{d}} = C_{\mathrm{D}}\sqrt{\frac{(\mathrm{d}E)^3}{E_{\mathrm{exit}}}} \end{cases} \tag{20}$$

where C_W and C_{D} are coefficients describing the dependence on all other parameters.

Data availability statement

The data cannot be made publicly available upon publication because they are not available in a format that is sufficiently accessible or reusable by other researchers. The data that support the findings of this study are available upon reasonable request from the authors.

Acknowledgments

This work was supported by the UK Engineering Physical Sciences Research Council, Grants EP/K040359/1 and EP/R029075/1, the National Research Foundation of South Africa and The South African Quantum Technology Initiative (SA QuTI). J A M acknowledges a UKRI Future Leaders Fellowship, Grant No. MR/X023125/1. E P is grateful to the Azrieli foundation for the award of an Azrieli fellowship.

Code availability

The code employed to generate the simulations presented in this work, as well as the data analysis code are available upon request. Interested parties may inquire about access to the code by contacting the corresponding author.

Conflict interests

The authors declare no competing interests.

Author contributions

E P developed the theoretical model, produced data plots, interpreted the data and contributed to the drafting of the paper. M D B ran the experiment, carried out the simulation work, interpreted the data and contributed to the drafting of the paper. Both E P and M D B contributed equally. H H designed, processed the devices and assisted with measurements. J A M contributed to data interpretation. T M carried out the e-beam lithography. H E B and D A R developed and grew the GaAs/AlGaAs heterostructures used. M P provided support, references, and useful discussions.

ORCID iDs

E Pyurbeeva 0000-0002-5521-4458
M D Blumenthal 0000-0002-1410-1860
J A Mol 0000-0003-0411-2598
D A Ritchie 0000-0002-9844-8350
M Pepper 0000-0003-3052-5425

References

[1] Pekola J P, Saira O-P, Maisi V F, Kemppinen A, Mottonen M, Pashkin Y A and Averin D V 2013 Single-electron current sources: toward a refined definition of the ampere *Rev. Mod. Phys.* **85** 1421–72

[2] Keller M, Martinis J, Steinbach A and Zimmerman N 1997 A seven-junction electron pump: design, fabrication and operation *Instrum. Meas. IEEE Trans.* **46** 307–10

[3] Bäuerle C, Christian Glattli D, Meunier T, Portier F, Roche P, Roulleau P, Takada S and Waintal X 2018 Coherent control of single electrons: a review of current progress *Rep. Prog. Phys.* **81** 056503

[4] Kaneko N-H, Nakamura S and Okazaki Y 2016 A review of the quantum current standard *Meas. Sci. Technol.* **27** 032001

[5] Dupont-Ferrier E, Roche B, Voisin B, Jehl X, Wacquez R, Vinet M, Sanquer M and De Franceschi S 2013 Coherent coupling of two dopants in a silicon nanowire probed by landau-zener-stückelberg interferometry *Phys. Rev. Lett.* **110** 136802

[6] DiVincenzo D and IBM 2000 The physical implementation of quantum computation *Fortschr. Phys.* **48** 771–83

[7] Wright S J, Blumenthal M D, Pepper M, Anderson D, Jones G A C, Nicoll C A and Ritchie D A 2009 Parallel quantized charge pumping *Phys. Rev. B* **80** 113303

[8] Maisi V, Pashkin Y, Kafanov S, Tsai J-S and Pekola J 2009 Parallel pumping of electrons *New J. Phys.* **11** 113057

[9] Giblin S P, Fujiwara A, Yamahata G, Bae M-H, Kim N, Rossi A, Möttönen M and Kataoka M 2019 Evidence for universality of tunable-barrier electron pumps *Metrologia* **56** 044004

[10] Yamamoto M, Takada S, Bäuerle C, Watanabe K, Wieck A D and Tarucha S 2012 Electrical control of a solid-state flying qubit *Nat. Nanotechnol.* **7** 247–51

[11] Ji Y, Chung Y, Sprinzak D, Heiblum M, Mahalu D and Shtrikman H 2003 An electronic mach–zehnder interferometer *Nature* **422** 415–8

[12] Ubbelohde N, Hohls F, Kashcheyevs V, Wagner T, Fricke L, Kästner B, Pierz K, Schumacher H W and Haug R J 2015 Partitioning of on-demand electron pairs *Nat. Nanotechnol.* **10** 46–49

[13] Gumbs G, Huang D, Blumenthal M, Wright S J, Pepper M and Abranyos Y 2009 Spin-split excitation gap and spin entanglement of a pair of interacting electrons in a quantum dot *Semicond. Sci. Technol.* **24** 115001

[14] Fletcher J D *et al* 2013 Clock-controlled emission of single-electron rightave packets in a solid-state circuit *Phys. Rev. Lett.* **111** 216807

[15] Kaestner B and Kashcheyevs V 2015 Non-adiabatic quantized charge pumping with tunable-barrier quantum dots: a review of current progress *Reports Prog. Phys.* **78** 103901

[16] Ubbelohde N *et al* 2023 Two electrons interacting at a mesoscopic beam splitter *Nat. Nanotechnol.* **18** 733–40

[17] Brange F and Flindt C 2023 Interacting electrons collide at a beam splitter *Nat. Nanotechnol.* **18** 696–7

[18] Blumenthal M D, Kaestner B, Li L, Giblin S, Janssen T J B M, Pepper M, Anderson D, Jones G and Ritchie D A 2007 Gigahertz quantized charge pumping *Nat. Phys.* **3** 343–7

[19] Kaestner B *et al* 2008 Single-parameter nonadiabatic quantized charge pumping *Phys. Rev. B* **77** 153301

[20] Rossi A, Tanttu T, Tan K Y, Iisakka I, Zhao R, Chan K W, Tettamanzi G C, Rogge S, Dzurak A S and Möttönen M 2014 An accurate single-electron pump based on a highly tunable silicon quantum dot *Nano Lett.* **14** 3405–11

[21] Yamahata G, Nishiguchi K and Fujiwara A 2014 Gigahertz single-trap electron pumps in silicon *Nat. Commun.* **5** 5038

[22] Schupp F J 2017 Single-electron devices in silicon *Mater. Sci. Technol.* **33** 944–62

[23] Giblin S P, Yamahata G, Fujiwara A and Kataoka M 2023 Precision measurement of an electron pump at 2GHz; the frontier of small dc current metrology *Metrologia* **60** 055001

[24] Blumenthal M D, Mahony D, Ahmad S, Gouveia D, Howe H, Beere H E, Mitchel T, Ritchie D A and Pepper M 2023 Multiple electron pumping *EPJ Quantum Technol.* **10** 46

[25] Stein F *ea tl* 2016 Robustness of single-electron pumps at sub-ppm current accuracy level *Metrologia* **54** S1

[26] Giblin S P, Bae M-H, Kim N, Ahn Y-H and Kataoka M 2017 Robust operation of a GaAs tunable barrier electron pump *Metrologia* **54** 299

[27] Giblin S P, Mykkönen E, Kemppinen A, Immonen P, Manninen A, Jenei M, Möttönen M, Yamahata G, Fujiwara A and Kataoka M 2020 Realisation of a quantum current standard at liquid helium temperature with sub-ppm reproducibility *Metrologia* **57** 025013

[28] Yamahata G and Fujiwara A 2024 An ambipolar single-charge pump in silicon *Appl. Phys. Lett.* **125** 163502

[29] Schoinas N *et al* 2024 Fast characterization of multiplexed single-electron pumps with machine learning *Appl. Phys. Lett.* **125** 124001

[30] Kashcheyevs V and Kaestner B 2010 Universal decay cascade model for dynamic quantum dot initialization *Phys. Rev. Lett.* **104** 1–4

[31] Howe H, Blumenthal M, Beere H E, Mitchell T, Ritchie D A and Pepper M 2021 Single-electron pump with highly controllable plateaus *Appl. Phys. Lett.* **119** 153102

[32] Rossi A, Klochan J, Timoshenko J, Hudson F E, Möttönen M, Rogge S, Dzurak A S, Kashcheyevs V and Tettamanzi G C 2018 Gigahertz single-electron pumping mediated by parasitic states *Nano Lett.* **18** 4141–7

[33] Wright S J *et al* 2008 Enhanced current quantization in high-frequency electron pumps in a perpendicular magnetic field *Phys. Rev. B* **78** 1–4

[34] Kaestner B, Leicht C, Kashcheyevs V, Pierz K, Siegner U and Schumacher H W 2009 Single-parameter quantized charge pumping in high magnetic fields *Appl. Phys. Lett.* **94** 012106

[35] Leicht C, Kaestner B, Kashcheyevs V, Mirovsky P, Weimann T, Pierz K and Schumacher H W 2010 Non-adiabatic pumping of single electrons affected by magnetic fields *Physica E* **42** 911–4

[36] Fletcher J D *et al* 2012 Stabilization of single-electron pumps by high magnetic fields *Phys. Rev. B* **86** 155311

[37] Hanief N, Blumenthal M, Howe H, Beere H, Mitchell T, Ritchie D and Pepper M 2024 Comparative study of low magnetic field effects in finger-finger and finger-split gate single electron pumps *Sci. Afr.* **24** e02150

[38] Leicht C, Mirovsky P, Kaestner B, Hohls F, Kashcheyevs V, Kurganova E V, Zeitler U, Weimann T, Pierz K and Schumacher H W 2011 Generation of energy selective excitations in quantum hall edge states *Semicond. Sci. Technol.* **26** 055010

[39] Kataoka M, Fletcher J D, See P, Giblin S P, Janssen T J, Griffiths J P, Jones G A, Farrer I and Ritchie D A 2011 Tunable nonadiabatic excitation in a single-electron quantum dot *Phys. Rev. Lett.* **106** 126801

[40] Wright S *et al* 2010 Single- and few-electron dynamic quantum dots in a perpendicular magnetic field *J. Appl. Phys.* **109** 102422

[41] Ryan J M, Deutscher N F and Ferry D K 1993 Gated-region transport in the quantum hall effect *Phys. Rev. B* **48** 8840–7

[42] Pyurbeeva E, Mol J A and Gehring P 2022 Electronic measurements of entropy in meso- and nanoscale systems *Chem. Phys. Rev.* **3** 041308

[43] Pyurbeeva E, Thomas J O and Mol J A 2023 Non-equilibrium thermodynamics in a single-molecule quantum system *Mater. Quantum Technol.* **3** 025003

[44] Juergens S, Haupt F, Moskalets M and Splettstoesser J 2013 Thermoelectric performance of a driven double quantum dot *Phys. Rev. B* **87** 1–14

[45] Hino Y and Hayakawa H 2021 Geometrical formulation of adiabatic pumping as a heat engine *Phys. Rev. Res.* **3** 013187

[46] Monsel J, Schulenborg J, Baquet T and Splettstoesser J 2022 Geometric energy transport and refrigeration with driven quantum dots *Phys. Rev. B* **106** 035405

[47] Monsel J, Schulenborg J and Splettstoesser J 2023 Non-geometric pumping effects on the performance of interacting quantum-dot heat engines *Eur. Phys. J. Spec. Top.* **123** 3267–72

[48] Kashcheyevs V and Timoshenko J 2012 Quantum fluctuations and coherence in high-precision single-electron capture *Phys. Rev. Lett.* **109** 216801

[49] Kashcheyevs V and Timoshenko J 2014 Modeling of a tunable-barrier non-adiabatic electron pump beyond the decay cascade model *CPEM Dig.* (*Conf. Precis. Electromagn. Meas.*) pp 536–7

[50] Fricke L *et al* 2013 Counting statistics for electron capture in a dynamic quantum dot *Phys. Rev. Lett.* **110** 126803

[51] Yamahata G, Johnson N and Fujiwara A 2021 Understanding the mechanism of tunable-barrier single-electron pumping: mechanism crossover and optimal accuracy *Phys. Rev. B* **103** 245306

[52] Hohls F, Kashcheyevs V, Stein F, Wenz T, Kaestner B and Schumacher H W 2022 Controlling the error mechanism in a tunable-barrier nonadiabatic charge pump by dynamic gate compensation *Phys. Rev. B* **105** 205425

[53] Zimmerman N M, Hourdakis E, Ono Y, Fujiwara A and Takahashi Y 2004 Error mechanisms and rates in tunable-barrier single-electron turnstiles and charge-coupled devices *J. Appl. Phys.* **96** 5254–66

[54] Schulenborg J, Fletcher J D, Kataoka M and Splettstoesser J 2024 Spectroscopy of hot-electron pair emission from a driven quantum dot *Phys. Rev. B* **109** 115433

[55] Beenakker C W J 1991 Theory of Coulomb-blockade oscillations in the conductance of a quantum dot *Phys. Rev. B* **44** 1646–56

[56] Davies J H 1997 *The Physics of Low-Dimensional Semiconductors: An Introduction* (Cambridge University Press)

[57] Qian Q, Nakamura J, Fallahi S, Gardner G C, Watson J D, Lüscher S, Folk J A, Csáthy G A and Manfra M J 2017 Quantum lifetime in ultrahigh quality GaAs quantum wells: relationship to $\Delta_{5/2}$ and impact of density fluctuations *Phys. Rev. B* **96** 035309

[58] Dmowski L H, Zduniak A, Litwin-Staszewska E, Contreras S, Knap W and Robert J L 1996 Study of quantum and classical scattering times in pseudomorphic algaas/ingaas/gaas by means of pressure *Phys. Status Solidi b* **198** 283–8

[59] Manfra M J, Simon S H, Baldwin K W, Sergent A M, West K W, Molnar R J and Caissie J 2004 Quantum and transport lifetimes in a tunable low-density algan/gan two-dimensional electron gas *Appl. Phys. Lett.* **85** 5278–80

[60] Wang D Q, Chen J C H, Klochan O, Das Gupta K, Reuter D, Wieck A D, Ritchie D A and Hamilton A R 2013 Influence of surface states on quantum and transport lifetimes in high-quality undoped heterostructures *Phys. Rev. B* **87** 195313

[61] Fujiwara A, Zimmerman N M, Ono Y and Takahashi Y 2004 Current quantization due to single-electron transfer in Si-wire charge-coupled devices *Appl. Phys. Lett.* **84** 1323–5

[62] Fujiwara A, Nishiguchi K and Ono Y 2008 Nanoampere charge pump by single-electron ratchet using silicon nanowire metal-oxide-semiconductor field-effect transistor *Appl. Phys. Lett.* **92** 042102